

Characterization of Hybrid Pixel Detector With CdTe Sensor

L. B. Rosa,^{a,b,*} L. H. Mendes,^{a,b} R. A. Negro de Oliveira,^a G. Paulino,^a S. M. Santos,^a R. P. Tartarotti,^a P. H. Oliveira,^a T. Barbosa^a and A. Tomal^b

^a*Pitec*

Campinas-SP, Brazil

^b*Gleb Wataghin Institute of Physics, University of Campinas, UNICAMP,
Campinas-SP, Brazil*

E-mail: leticia.rosa@pitec.co, lrosa@ifi.unicamp.br

The X-ray techniques used in synchrotron sources have been an indispensable tool in studying the physical aspects of various fields, such as biology, chemistry, and materials science. The results of these experiments often depend on the performance of the detectors, especially when studying sample dynamics, which require fast and sensitive X-ray detectors. This work presents a description of the PIMEGA X-ray camera system based on 1 mm thick CdTe sensors with a 55 μm pixel pitch bump-bonded to Medipix3RX ASICs. It is also described the preliminary results of the system's prototype characterization and imaging capabilities, which were conducted in terms of spatial resolution, detective quantum efficiency, leakage current, full depletion, and equalization responses. The experiments were performed using the detector in super high gain mode, with a 12-bit configuration in Fine Pitch and Single-Pixel mode. The results show the high-quality imaging capabilities of the detector with excellent values of MTF and DQE.

*10th International Workshop on Semiconductor Pixel Detectors for Particles and Imaging (Pixel2022)
12-16 December 2022
Santa Fe, New Mexico, USA*

*Speaker

1. Introduction

Synchrotron X-ray techniques have been a valuable tool in probing physical aspects and dynamics of processes in various fields of research, such as biology, chemistry, and material science, for many decades [1, 2]. These techniques rely on the use of high-intensity X-rays generated at synchrotron light sources, which provide a unique and powerful tool for investigating the structure and properties of materials and biological systems. The high-resolution, high-speed imaging capabilities of hybrid-pixel detectors, combined with the unique properties of synchrotron X-rays, make this a valuable tool for advancing knowledge in various fields of research [1].

Over the past few decades, the advance of coherent X-ray imaging has been boosted by the creation of brighter light sources and phase-retrieval techniques [3, 4]. These techniques allow the recovery of the complex amplitude scattered by a sample that has been illuminated with coherent light. Currently, the resolution of coherent diffracting imaging, with both hard and soft X-rays, extends beyond the nanometer scale [5]. This is made possible due to the 4th generation light sources, which produce high-quality coherent X-ray flux, making them ideal for supporting these imaging techniques [1–4]. It was required to push the boundaries of detector technology toward sensors capable of counting photons at higher rates and in a broader energy range. For that reason, materials with high atomic numbers Z , such as Gallium Arsenide (GaAs) [6], Cadmium Telluride (CdTe) [7, 8], and Cadmium Zinc Telluride (CdZnTe) [9] were introduced to provide those features and enhance the experiment capabilities [10].

Today, due to their great data acquisition speed and flexibility, semiconductor hybrid photon-counting detectors are the technology of choice in many research fields - *e.g.*, particle physics, heavy ion nuclear collision, and X-ray synchrotron experiments, where different requirements are needed - therefore having an important role in scientific research throughout several areas. In particular, these detectors can be used in various synchrotron applications, including Powder Diffraction (XPD) [11], Macro-molecular Crystallography, Bragg coherent X-ray diffraction, Small-Angle X-Ray Scattering (SAXS), Wide-Angle X-Ray Scattering (WAXS), Grazing-Incidence Small-Angle Scattering (GISAXS), Micro and Nano-Tomography [3, 5], Ptychographic X-Ray computed tomography (PXCT) [3, 5], and X-Ray Photon Correlation Spectroscopy (XPCS).

By utilizing a high- Z semiconductor instead of silicon, a hybrid photon counting detector can achieve efficient hard X-ray absorption while retaining its advantages [12, 13]. The PIMEGA detector system has been developed to be compatible with high- Z materials, and compact prototype PIMEGA systems based on Cadmium Telluride (CdTe) have been built. In this work, an overview of the PIMEGA CdTe detector and its unique features are shown. We also present the detector characteristics, and measurements on Modulation Transfer Function (MTF), and Detective Quantum Efficiency (DQE). In addition, to demonstrate the PIMEGA's capabilities for biological imaging applications, a large area, low noise, and a high-resolution image of a biological sample are also reported.

2. PIMEGA System Overview

PIMEGA is a modular family of X-ray cameras designed to fulfill the highly demanding requirements of a 4th generation synchrotron source, providing high-speed acquisition and low-noise imaging with small pixel size and excellent spatial resolution with minimum dead area. The X-ray sensors are made with the proven and widely used hybrid pixel photon-counting technology based on Medipix3RX ASIC [14], capable to achieve a high frame rate, faster readout time, and continuous read and write mode. These detectors have the advantage of $55 \times 55 \mu\text{m}^2$ pixel size and can reach a frame rate of up to 2000 frames per second and a configurable dynamic range of 12 or 24 bits of depth range. The adjustable energy threshold allows for the detector to operate with minimum intrinsic noise, resulting in better signal-to-noise ratio characteristics.

2.1 Overall Design

The PIMEGA mechanical design is made of sensor module elements named Hexa-modules, in which one monolithic Si sensor is bump bonded to six Medipix3RX. For the assembly of the prototype, an adaptation was created using six individual CdTe sensors, each connected to six Medipix3RX ASICs with 256×256 pixels. The ASICs are positioned close together with a small gap between adjacent pixels on the ASIC edge. The sensor module is glued to a thermal mechanism and then attached to a stainless steel heat spreader to remove heat generated by the ASICs.

The detector sensor head is modular, and it is designed in such a way that can accommodate 6 Hexa-modules in an arrangement of 6×6 ASICs. The Medipix3RX are then wire bonded to a board which in turn is attached to a flexible cable responsible for carrying out the electric connections, providing power for the semiconductor sensors, and routing to the Medipix ASIC signals. Figure 1a shows the mechanical design of a PIMEGA camera with 6 Hexa-modules named PIMEGA 135D.

The readout boards, *i.e.*, Medipix Board (MB), connect to the sensor modules in a way that allows the readout electronics to fit behind the detector modules, enabling multiple modules to be placed together covering large areas. In such a design, each MB is able to obtain the data from two Hexa-modules. Finally, the mounting chassis is responsible for providing the required mechanical stability and accurate positioning of the monolithic sensor modules.

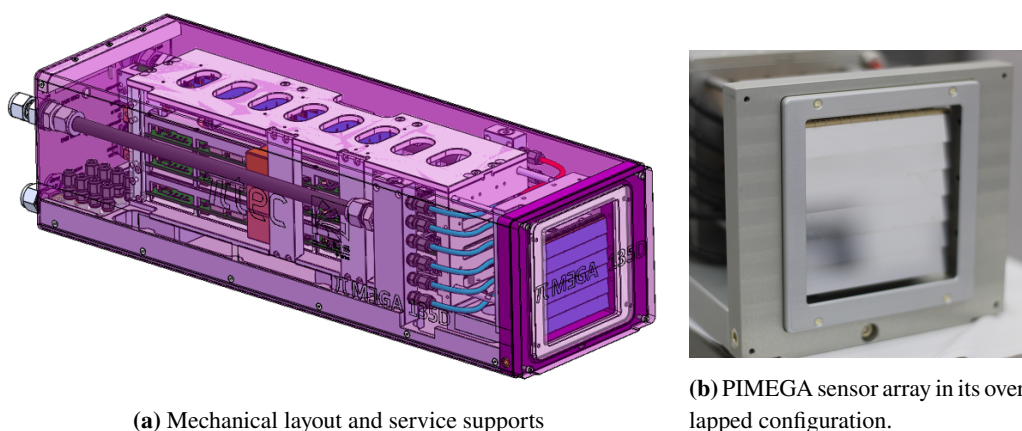


Figure 1: PIMEGA 135D detector design.

Since for full-frame readout mode, the Medipix3RX consumes about 1 W [15], then it adds up to 6 W in total for each sensor module. In order to dissipate such power, each water-cooled heat-spreader is attached to a manifold which is connected to a cooling plant or chiller through stainless steel tubes. The cooling plant provides the cooling water needed to cool down the sensors and keep the detector temperature inside the operating range.

Finally, due to the combination of its unique design features, the detector is low vacuum compatible and it can operate in pressures under 10^{-3} mbar, extending the capabilities of the system to low energy X-ray applications, where the X-ray photon absorption by the air is a critical issue.

2.2 Data Interface

The communication with the user's workstation computer is carried through a 100 Gbps Ethernet fiber optical link by sending commands requesting data reading or writing, by using encoded remote procedure calls. In this same medium in which the commands are sent for control and configuration, data transmission is also carried out at very high speed for the acquired high-resolution images.

Two implementations must be considered, the front-end electronics (detector side, that transmits data stream) and a back-end workstation (receiving side). Usual data destinations are circular buffers implemented in the random-access memory (RAM). Other possible destinations are graphics processing units (GPU), coprocessors, and disk controllers.

The Remote Direct Memory Access (RDMA) protocols consist of transferring data from memory from one device to another without any central processing unit (CPU) intervention, enabling high throughput and low latency. With RDMA protocol, the CPU on the workstation will handle only the flow control, requesting transfers and receiving events indicating completion, while the encapsulation and processing of the packets are delegated to the network interface card (NIC) or to the embedded Field Programmable Gate Array (FPGA).

For comparison with the Open Systems Interconnection (OSI) model, TCP/IP Ethernet is a transport byte-stream oriented for passing information in bytes between socket applications. It is designed with losses but implements a reliability scheme using the transmission control protocol (TCP), which requires operating system intervention for every operation including copying the buffer, which adds latency and consumes memory and CPU resources [16].

In InfiniBand (IB) standard, a complete message is sent directly to an application. Once an application has requested to transport an RDMA read or write, the IB hardware segments the outgoing message as needed into packets. These packets are transmitted over the IB network and delivered directly to the receiving application's virtual buffer, where they are reassembled into a complete message. The receiving application is notified once the entire message has been received. Therefore, neither the sending nor the receiving application is involved until the entire message has been delivered to the receiving application's buffer, and this is a great advantage since it allows the CPU offload.

RDMA over Converged Ethernet (RoCE) protocol is an InfiniBand Trade Association (IBTA) standard designed to provide InfiniBand transport services over Ethernet networks. RoCE preserves the semantics of InfiniBand verbs along with their transport and network protocols and replaces the InfiniBand link and physical layers with Ethernet. The network management infrastructure for

RoCE is also Ethernet, and in this way the packets can be transparently forwarded by Ethernet switches [17].

The data flow of the PIMEGA system is implemented using the mentioned protocols and an example schematic is shown in Figure 2. Through the RoCE protocol, data is received at a rate of up to 2000 frames per second. The workstation computer provides the role of a server for a distributed control system that supports the Experimental Physics and Industrial Control System (EPICS) framework [18].

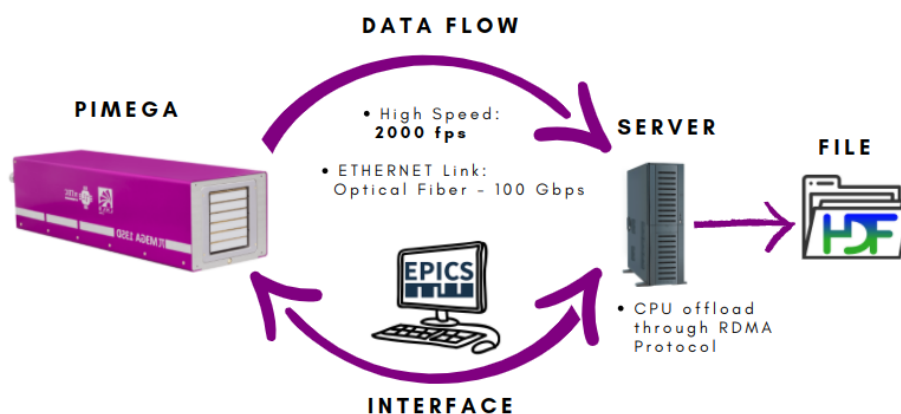


Figure 2: PIMEGA data flow architecture.

2.3 Detector Control and Software

The PIMEGA Software Suite (PSS), a collection of related programs compliant with the EPICS, manages the detector's control, status, and acquisition. The PSS processes the incoming frame on a Linux server, transforming it into a raw image. It is then subjected to image processing algorithms to produce the final image for visualization. The detector can be remotely controlled by the EPICS framework or locally on the server. The modules included in the PSS are:

- Graphical User Interface (GUI): Application that allows the end user to run X-ray experiments and acquire images;
- Command-Line Interface (CLI): Application designed to enable both basic and advanced users to operate X-ray imaging equipment. Basic users are able to utilize fundamental commands for acquiring images, while advanced users have access to more complex commands that allow them to configure the detector to their specific needs;
- Software Development Kit (SDK): A set of modules that offer essential functionalities and interfaces for operating and testing the detector, including an EPICS driver, Python Tools and Wrapper, and an Application Programming Interface (API). The detector can be controlled locally through a Linux server or remotely via Ethernet using the API and EPICS driver;
- Camera System: A high-performance backend module that processes and saves the data generated by the front-end detector. This module can operate using either a CPU or a GPU for faster processing;

- **Image Viewer:** A tool for image visualization that enables data processing and near-real-time viewing at a frame rate suitable for human perception. The data can be stored in various formats, including HDF5, EDF, TIFF, and JPEG.

Using the EPICS driver, the detector is connected to the EPICS framework, which allows it to be used in a control system with many other devices, such as motors, and measurement systems, making it possible to synchronize the devices in action. Figure 3 illustrates a high-level block diagram of the PSS software architecture.

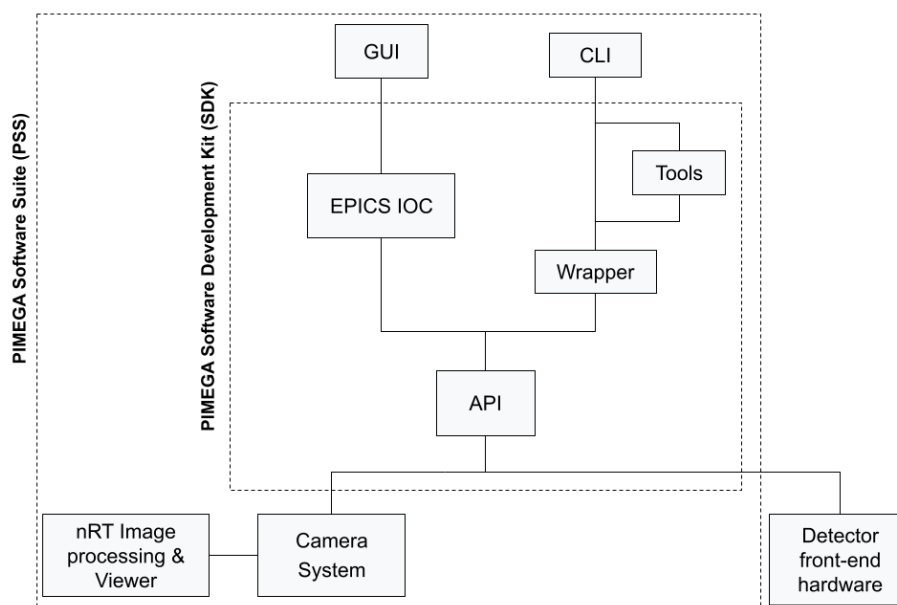


Figure 3: PIMEGA Software Suite architecture.

2.3.1 Detector Configuration

In order to ensure the proper functioning of the analog circuit, the digital-to-analog converters (DACs) output voltage values must be within their recommended range. This is achieved through a process called DAC Scan, which involves setting a digital value, reading the corresponding analog value, and then setting a specific analog value as defined by the user. In the DAC Scan process, the GND, FBK, and CAS DACs are optimized by default, with their optimal analog values set to 650 mV, 900 mV, and 850 mV, respectively.

After adjusting the DACs, it is important to minimize the threshold dispersion among pixels in terms of the relationship between threshold and energy, which can be caused by transistor mismatch during chip fabrication, through a process called equalization. To minimize this difference, each Medipix3RX discriminator has a 5-bit current DAC (ConfigDiscL and ConfigDiscH) that can shift the threshold positively or negatively, depending on the selected digital code, and a global 8-bit DAC (DiscL and DiscH) that sets the global dynamic range of the threshold values within the 5-bit adjustment DAC. The equalization algorithm was based on previous work described in [19].

3. Experiment and Characterization Results

3.1 Experimental Setup

The experiments presented in this study were carried out with a prototype of PIMEGA detector composed of a sensor module of 1 mm thickness CdTe sensor. A scheme of the detector used is shown in Figure 4a. The polychromatic radiation source used to irradiate the detector was a commercial X-ray tube with a Tungsten target at 70 kV and a 3 mm additional aluminum filter.

The high voltage powering scheme of the CdTe detector is a crucial component of the system and its operating safety. For this application, a new high-voltage power scheme was designed to provide high flexibility for the adjustment of the bias voltages depending on the individual characteristics of each sensor module, improving the detector efficiency and stability. For the prototype used in this work, the power supply is external and is installed along with patch panels from which a single voltage cable is connected to the detector. This power supply scheme is responsible to provide 12 V and the required power for the readout electronic boards.

The detector was characterized in terms of leakage current, full depletion response, spatial resolution, and detective quantum efficiency. All measurements presented in this work were performed with the detector operating in super high gain mode and 12-bit configured in Fine Pitch and Single Pixel Mode. Previous to all measurements, a DAC optimization routine was performed along with an equalization procedure necessary to reduce variations among the pixel's responses to energy thresholds.

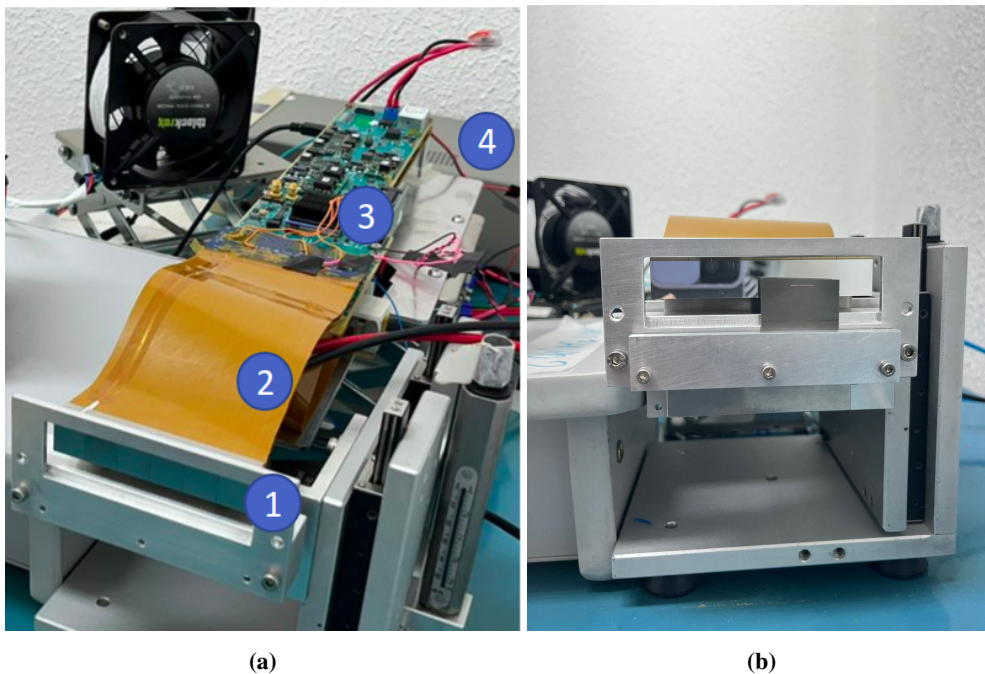
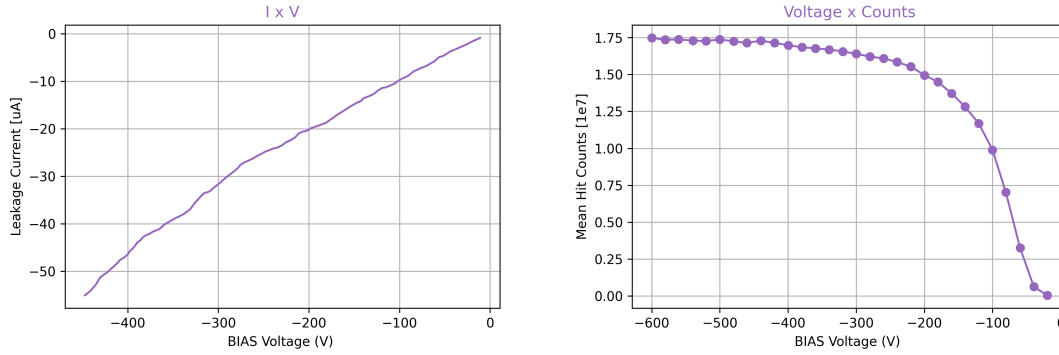


Figure 4: Experimental setup (a) PIMEGA camera system prototype; 1 - CdTe sensors; 2 - Flexible cable connection; 3 - Medipix Board; 4 - High-voltage power supply and (b) Slanted edge Tungsten object for MTF acquisition and scanning mechanism.

3.2 Leakage Current and Full Depletion

The detector was biased at different voltages through the high-voltage power supply enabling the measurement of the leakage current in the sensor module sensors, as shown in Figure 5a, where the current was measured 2 minutes after each voltage was set. The applied bias was set in negative polarity, which stands for electron collection in CdTe.

The count rate in the sensor module as a function of the bias voltage is shown in Figure 5b, where one can see that the full depletion range is reached for bias voltages exceeding about -200 V. Therefore, it was chosen the bias voltage of -250 V to operate the detector throughout all the measurements [15, 20, 21].



(a) Leakage current as a function of the applied bias in CdTe (b) Mean value of hit counts in sensor module sensors versus negative bias voltage applied.

Figure 5: Bias dependency on PIMEGA CdTe sensor module sensors.

3.3 Equalization

To equalize the detector, the dispersion between pixels must be measured, which can be accomplished by using either the electronic noise floor, X-ray, or test pulses simulating real photon-generated current as input signals. In this paper, the first method was selected due to its speed and efficiency. The 5-bit DACs (ConfigDiscL and ConfigDiscH) are configured with at least two distinct values for all pixels. Then, a threshold scan is executed, which consists of varying the threshold DAC value and making an image acquisition. The obtained curves were then evaluated to determine the optimal adjustment value for each pixel in order to achieve the desired noise target.

As presented in Figure 6a, the threshold scan of an unequalized chip shows a significant dispersion between pixels, resulting in a curve that conforms to a Gaussian distribution. After the threshold trimming, there is a reduction in the dispersion, and the electronic noise floor is concentrated at low threshold values, – *i.e.*, low energies – close to the selected target of 10, as shown in Figure 6b.

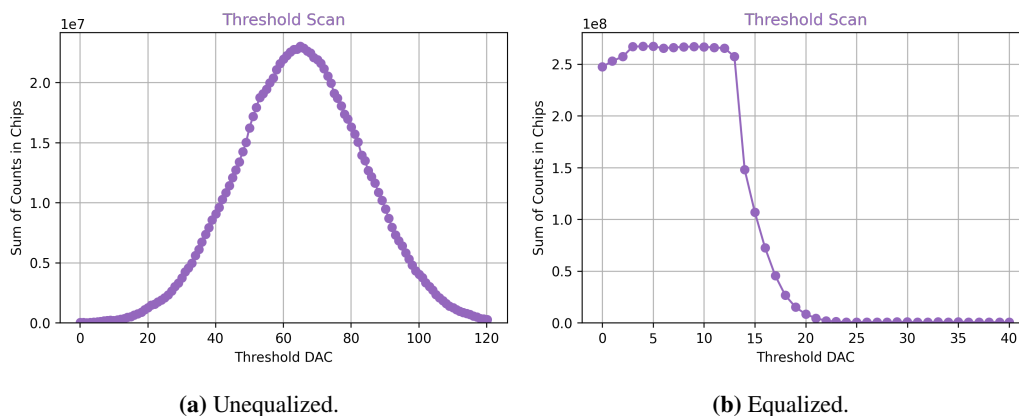


Figure 6: Threshold Scan for a chip.

3.4 MTF and DQE Metrics

The Modulation Transfer Function (MTF) is an important metric that represents how well the system preserves the spatial frequency content of an object in the recorded image. High MTF values correspond to high contrast and sharpness in the image, and low MTF values indicate that the system blurs or loses fine details in the object. MTF is used to analyze the spatial resolution response of the detector as a function of the frequency of the input signal.

In this work, the MTF was measured with the standard slanted-edge technique [22] by recording images of a slanted tungsten edge positioned close to the detector surface at approximately 2.5 degrees to a sensor row, as shown in Figure 4b and similarly performed previously for PIMEGA Si detector [23]. In order to determine the MTF, images of the radiopaque tungsten object with the slanted edge were acquired using the X-ray tube set at 70 kV and 50 mAs at a distance of 1.6 m, which corresponds to a radiation dose of 284.47 μ Gy. The line spread function (LSF) is extracted from the edge spread function profile (ESF) and then the transfer function is obtained through a normalized Fourier transformation [24]. Figure 7 shows the image of the edge acquired.

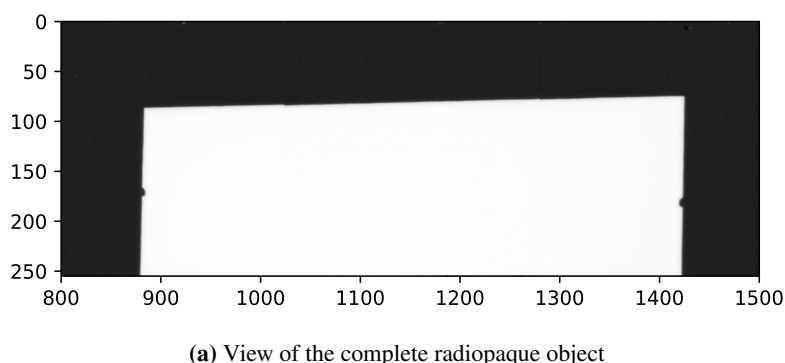
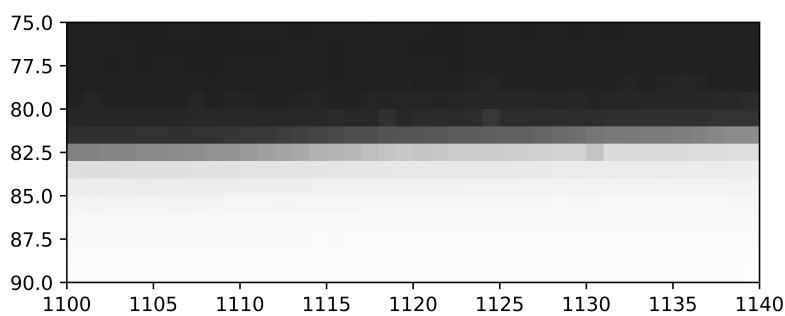


Figure 7: Tungstein slanted edge image acquired for MTF with PIMEGA system (part 1 of 2).

POS(Pixel2022)057



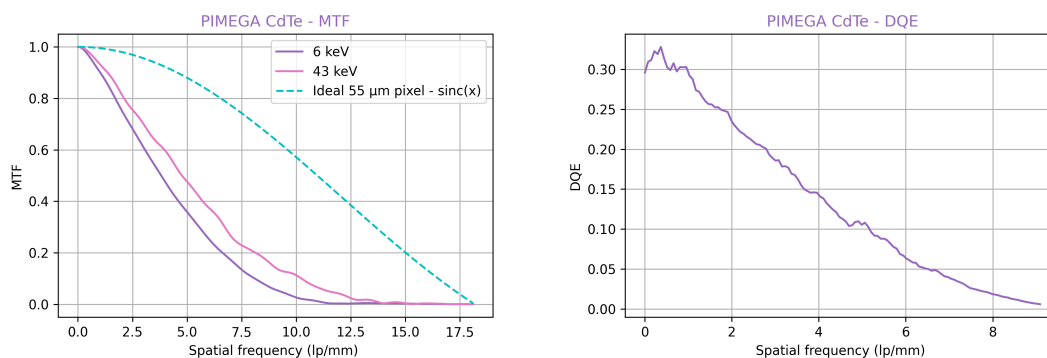
(b) Zoom in the slanted edge profile transition region.

Figure 7: Tungstein slanted edge image acquired for MTF with PIMEGA system (part 2 of 2).

Figure 8a shows the MTF as a function of the spatial frequency. The energy threshold was set to a noise level of 6 keV and a bit above half of the incident maximum energy at about 43 keV. The Nyquist frequency is given by [25]:

$$N_y = \frac{1}{2 \times p} \quad , \quad (1)$$

where p is the pixel pitch that in this case is $55 \mu\text{m}$, resulting in a Nyquist frequency of 9.09 lp/mm . The spatial resolution given by MTF at 0.3 was found to be 5.51 lp/mm for 6 keV and 6.74 lp/mm for 43 keV. MTF was found to be better when increasing the detector's energy threshold, which means a minimization in the charge shared among adjacent pixels occurs due to the reduction in the effective pixel size.



(a) MTF dependence on detector's energy threshold.

(b) Detector detective quantum efficiency.

Figure 8: PIMEGA CdTe (a) MTF curves computed from the experimental image acquired and the theoretical result for a squared-pixel detector, based on the Cardinal Sinus, and (b) the DQE curve obtained for the sensors measured in the same condition as the MTF.

Detective Quantum Efficiency (DQE) is a metric used to evaluate the performance of an imaging system, such as a digital X-ray detector, in terms of its ability to detect and preserve signal information. It quantifies the detection efficiency as a function of spatial frequency, and it can be calculated as [26]:

$$DQE(\nu) = \frac{MFT^2}{SNR_{in}^2 \times K \times NPS(\nu)}, \quad (2)$$

where K is the air kerma, SNR_{in}^2 is the squared signal-to-noise ratio per air kerma, and NPS is the Noise Power Spectrum (NPS) at the detector surface that quantifies the noise at different spatial frequencies. Finally, accordingly with Equation 2, the DQE was measured by recording a sequence of flat field images to calculate the NPS. Figure 8b shows the DQE values. It is important to point out that a higher DQE indicates a more efficient imaging system with lower noise and better signal-to-noise ratio characteristics. The obtained DQE for PIMEGA CdTe sensors presents a higher efficiency compared to other high-Z materials used in different photon-counting hybrid pixel detectors such as GaAs, as described previously in the literature [27].

3.5 X-ray Imaging

In addition to the MTF and DQE measurements, an imaging validation was performed to investigate and confirm the good performance of the PIMEGA CdTe detector system for small animal imaging with high resolution using a scanning mechanism that enables a larger detection area.

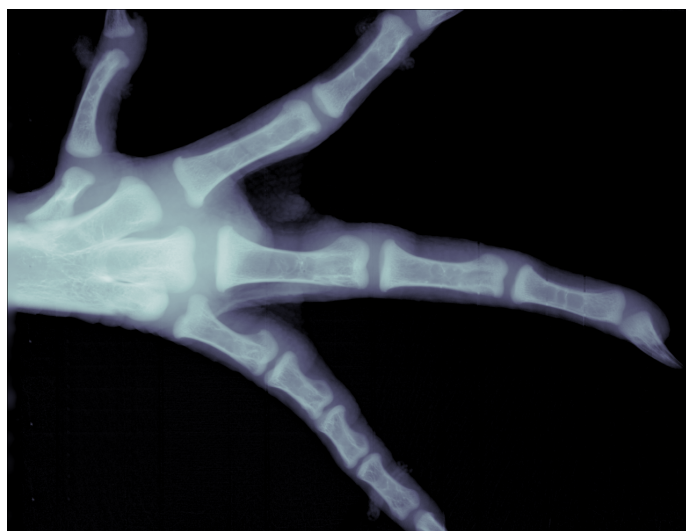


Figure 9: X-ray image of a poultry paw taken in multiple frames. In the image, the area covered is approximately 85 mm in length by 62 mm in height.

The X-ray image shown on Figure 9 was taken in multiple exposures – *i.e.*, acquired by scanning the sample with 2 sec. exposure time each – in single-pixel mode with the low energy threshold set to 6 keV, and the X-ray tube at 30 kV. Finally, a stitching reconstruction algorithm was applied along with flat field correction, to reconstruct the final image. In the image, it is possible to see with great detail the sub-millimeter features present on the poultry paw. It is also possible to clearly distinguish soft tissue from hard bone regions with excellent spatial resolution.

4. Summary and Future Work

A large-area photon-counting detector prototype of the PIMEGA 1 mm thick CdTe detector, with over 235 kpixel size and 55 μm pitch, was successfully assembled and commissioned. The detector demonstrates excellent imaging performance. It was verified that the high dynamic range and the noise-free detection combined with its low energy threshold enable a high contrast quality image as shown in the clear sample image of a poultry paw that was acquired with a scanning mechanism. The stitching reconstruction algorithm applied effectively reduced the impact of gaps between the ASICs, and the nonuniformities in the CdTe material were effectively addressed through flatfield correction.

The detector values of leakage current and full depletion voltage were measured, and the results are well in agreement with the results expected for a 1 mm CdTe sensor. The equalization procedure was performed on the CdTe prototype in accordance with standard procedure, resulting in a well-behaved, and functioning detector with low image noise. A good spatial resolution was achieved with MTF values as a function of the spatial frequency demonstrating high performance accordingly with expectations for a CdTe detector. Furthermore, the system presents a higher quantum efficiency compared to other high-Z materials.

Finally, the detector measurements demonstrate that the system is highly capable and suitable for a wide range of scientific experiments and X-ray imaging applications due to its low noise, fast time response, and excellent spatial resolution. Future work will include investigating and comparing the system behavior for Charge Summing Mode, also taking into consideration other operation biases, as well as performing a detailed characterization of the CdTe detector at high fluxes at a synchrotron beamline.

5. Acknowledgments

The authors would like to thank the Pitec team for supporting this work, especially members from the development group that gave assistance, and Filipe Cavalcanti for the careful revision. We are also grateful to the Sirius team for the constant collaboration and partnership, in particular, the LNLS Detector Group lead by Jean Polli. Furthermore, we acknowledge the important contributions of the Medipix collaboration.

References

- [1] J. Hill et al. *Future trends in synchrotron science at NSLS-II*. *J. Phys.: Condens. Matter* **32**, 374008 (20pp) (2020).
- [2] M.d.C. Fonseca et al. *High-resolution synchrotron-based X-ray microtomography as a tool to unveil the three-dimensional neuronal architecture of the brain*. *Sci Rep* **8**, 12074 (2018).
- [3] C. C. Polo et al. *Correlations between lignin content and structural robustness in plants revealed by X-ray ptychography*. *Sci Rep* **10**, 6023 (2020).
- [4] R. L. Headrick et al. *Coherent X-ray measurement of step-flow propagation during growth on polycrystalline thin film surfaces*. *Nat Commun* **10**, 2638 (2019).
- [5] H. C. N. Tolentino. et al. *X-ray microscopy developments at Sirius-LNLS: first commissioning experiments at the Carnauba beamline*. *Proc. SPIE, X-Ray Nanoimaging: Instruments and Methods V*. **118394**, (2021).
- [6] C. Schwarz et al. *Measurements with Si and GaAs pixel detectors bonded to photon counting readout chips*. *Nuclear Instruments and Methods in Physics Research Section A: Accelerators, Spectrometers, Detectors and Associated Equipment* **466**, 87–94 (2001).
- [7] M. Schütz, S. Procz, J. Fey, M. Fiederle. *Element discrimination via spectroscopic X-ray imaging with a CdTe medipix3rx detector*. *Journal of Instrumentation* **15**, (2020).
- [8] M. Khalil, E. S. Dreier, J. Kehres, J. Jakubek, and U. L. Olsen, *Subpixel resolution in CdTe timepix3 pixel detectors*. *Journal of Synchrotron Radiation* **25**, 1650–1657 (2018).
- [9] G. Roque et al. *Sub-pixel energy-weighting techniques for metallic contaminant highlighting in a pharmaceutical hard capsule using a timepix3 CdZnTe hybrid pixel detector*. *Journal of Instrumentation* **17**, (2022).
- [10] N. L. Archilha et al. *MOGNO, the nano and microtomography beamline at Sirius, the Brazilian synchrotron light source*. *J. Phys.: Conf. Ser.* **2380**, 012123 (2022).
- [11] F. R. Estrada et al. *PAINEIRA beamline at Sirius: an automated facility for polycrystalline XRD characterization*. *J. Phys.: Conf. Ser.* **2380**, 012033 (2022).
- [12] S. Kirschenmann et al. *Quality assessment of cadmium telluride as a detector material for multispectral medical imaging*. *Journal of Instrumentation* **17**, C01070 (2022).
- [13] S. Kirschenmann et al. *Multispectral photon-counting for medical imaging and beam characterization — A project review*. *Nuclear Instruments and Methods in Physics Research Section A: Accelerators, Spectrometers, Detectors and Associated Equipment*. **1039**, 167043 (2022).
- [14] R. Ballabriga et al., *The Medipix3RX: A high resolution, zero dead-time pixel detector readout chip allowing spectroscopic imaging*. *Journal of Instrumentation* **8** (2013).

- [15] E. Hamann et al., *Performance of a Medipix3RX Spectroscopic Pixel Detector With a High Resistivity Gallium Arsenide Sensor*. *IEEE Transactions on Medical Imaging* **34**, 707-715 (2015).
- [16] R. Recio et al., *RFC 5040: A Remote Direct Memory Access Protocol Specification*. (2007). Available at: <https://www.rfc-editor.org/rfc/rfc5040.html>. (Accessed: 28th January 2023)
- [17] InfiniBand Trade Association. *InfiniBand™ Architecture Specification Release 1.2.1 Annex A16: RoCE*. (2010).
- [18] EPICS - Experimental Physics and Industrial Control System. Available at: <https://epics-controls.org/> (Accessed: 28th January 2023)
- [19] J. Rinkel, D. Magalhães, F. Wagner, E. Frodij, and R. Ballabriga, *Equalization method for Medipix3RX*. *Nucl. Instrum. Methods Phys. Res. A* **801**, 1-6 (2015).
- [20] K.-F. G. Pfeiffer, *Evaluation of the MEDIPIX detectors for medical X-ray imaging, with special consideration of Mammography*. *Ph.D. Thesis, Univ. Erlangen-Nürnberg* (2004).
- [21] L. Rossi, P. Fischer, N. Wermes, and T. Rohe in *Pixel detectors: From fundamentals to applications*, Physica-Verlag 2006.
- [22] E. Samei, M. J. Flynn, and D. A. Reimann, *A method for measuring the presampled MTF of digital radiographic systems using an edge test device*. *Medical Physics* **25**, 102–113 (1998).
- [23] R. B. Campanelli, G. S. Gomes, M. G. Fernandes, L. H. Mendes, L. B. Rosa, R. C. Reis, E. B. Antonio, and J. M. Polli, *Large area Hybrid Detectors Based on Medipix3RX: Commissioning and Characterization at Sirius Beamlines* [Submitted for publication]. *Journal of Instrumentation* (2023).
- [24] R. S. Saunders Jr., E. Samei, J. L. Jesneck, and J. Y. Lo, *Physical characterization of a prototype selenium-based full-field digital mammography detector*. *Medical Physics* **32**, 588–599 (2005).
- [25] E. Samei, and D. J. Peck, *Hendee's Physics of Medical Imaging*. Wiley-Blackwell **106** (2019).
- [26] Medical electrical equipment - Characteristics of digital X-ray imaging devices - Part 1-1: Determination of the detective quantum efficiency - Detectors used in radiographic imaging. *IEC 62220-1-1:2015* (2015).
- [27] J. Scholz et al., *Biomedical x-ray imaging with a GaAs photon-counting detector: A comparative study*. *APL Photonics* **5** (2020).